Influence of the numerical schemes on the flow states of a simplified heavy vehicle

Turbulence, Heat and Mass Transfer 9

Influence of the numerical schemes on the flow states of a simplified heavy vehicle

A. Rao[1], J. Zhang[1], G. Minelli[1], B. Basara[2] and S. Krajnović[1,†]

[1]*Department of Mechanics and Maritime Sciences (M2), Chalmers University of Technology, Göteborg 41296, Sweden.* [†]*sinisa@chalmers.se*

[2]*AVL List GmbH, Advanced Simulation Technologies, Hans-List-Platz 1, 8020, Graz, Austria.*

Abstract — Recent experiments [1, 2] in the wake of a simplified heavy vehicle (also know as a ground transportation system (GTS)) have shown that the flow topology remains invariant over a large range of Reynolds numbers [$3.8 \times 10^4 - 2.8 \times 10^6$]. This allows numerical techniques such as large eddy simulations (LES) to accurately predict the flow topology at low Reynolds numbers. While LES requires grids of higher spatial resolution; hybrid RANS/LES turbulence models are an alternate choice, where, accurate prediction of the flow is possible on coarser grids ([3, 4]). Numerical simulations are performed using LES and a hybrid turbulence model - partially-averaged Navier–Stokes (PANS) equations at $Re_H = 3.8 \times 10^4$ for a unified tractor-trailer geometry to compare the flow topologies in the near wake. The influence of the numerical schemes on the flow topology in the symmetry plane which is susceptible to bi-stable flow is investigated using PANS, and compared with the results from LES.

1. Introduction

The Ground Transportation model (GTS) model is a simplified tractor-trailer ([2, 5]), with an elliptical rounded nose, a flat roof and underbody, and a squareback base. In the experimental investigations of [1, 2, 5], asymmetrical flow topology is observed in the vertical midplane of the body, while a pair of symmetrical counter-rotating vortices are observed in the lateral midplane in the near wake. In the vertical midplane, the flow field is characterised by a tiny vortex close to the base (A), adjoining a large triangular shaped vortex (B) and a smaller vortex (C) on the opposite side of vortex (B) - also see figures 1(a) and 1(b). Flow predictions using RANS fails to capture this asymmetrical flow topology, with a pair of symmetric vortices in both the lateral and the vertical midplanes ([6, 7]).

2. Numerical formulation, results and discussion

The LES and PANS equations are discretised in a commercial finite volume solver, AVL FIRE^{TM}2014, to solve the incompressible Navier–Stokes equations using a collocated grid arrangement. The numerical formulation has previously been validated for a wide range of bluff body flows ([8, 9, 10, 11, 12, 13]).

The flow field is investigated using both LES and PANS at $Re_H = 3.8 \times 10^4$ to compare directly with the experimental simulations of [1], where, Re_H is the Reynolds number based on the height of the GTS (H). The GTS is placed at a height of $0.14H$, as in the original studies of [2, 5]. For this study, two hexahedral meshes - $M1$ and $M2$ consisting of $\simeq$ 8.35 and $\simeq$ 10.8 million elements, respectively, are used. The boundaries of the computational domain are located at sufficiently far distances resulting in a blockage ratio of less than 1%. A time-step of $7.5 \times 10^{-4} s$ is used to ensure a CFL number ≤ 1. The averaging of the flow field is carried out after one flow

passage through the domain, for five flow passes. The averaged wall y-plus on the GTS was less than 0.5, with maximum wall y-plus being observed around the frontal corners, although never exceeding $y^+ = 2.5$. Four cases are investigated: Case I - LES using 95% central differencing scheme (CDS), Case II - PANS with AVL SMART (Sharp and Monotonic Algorithm for Realistic Transport), Case III - PANS with 95% CDS, and Case IV - PANS with 95% CDS. Mesh $M1$ is used for cases I-III, while mesh $M2$ is used for case IV. Shown in figure 1 are the contours of the time-averaged velocities for the four cases in the near wake. While the LES in Case I predicts a flow topology which is anti-symmetric to that observed in the experiments of [1, 2], Case II predicts a flow topology similar to the experiments, along with the formation of a ground vortex (D), which is nearly the height of the ground clearance. In Cases III and IV, the CDS schemes for the momentum equations produces a flow topology similar to the LES, but the recirculating region is elongated in the streamwise direction. With an increase in the spatial resolution in Case IV, the size of vortex C reduces as compared to case III (see figures 1(c) and 1(d)). The shape of the separatrix in Cases I, III and IV is different to Case II, with a more uniform curvature for the latter as a result of the upwash and the formation of the ground vortex (figure 1(b)). It may be recalled that the height-to-width ratio of the GTS (1.392) is similar to the width-to-height ratio of a squareback Ahmed body (1.35), where bi-stable flow is observed in the lateral midplane ([14, 15, 16, 17]). Thus, the two possible flow states are realised in the wake of the GTS, and the flow features with respect to mesh $M1$ for cases I and II are discussed with the aid of figure 2.

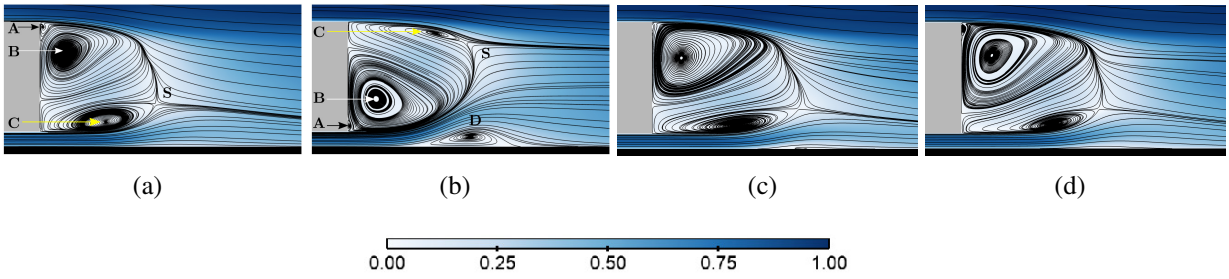

(a) (b) (c) (d)

Figure 1: Visualisation of the contours of the normalised time-averaged velocity in the vertical midplane at the rear of the GTS overlaid with streamlines. (a) Case I, (b) Case II, (c) Case III, and (d) Case IV. Flow is from left to right in these images. The predominant vortices are annotated by letters A-D, and the saddle point by letter S.

Shown in figures 2(a) and 2(d) are the contours of the pressure coefficient (C_p) on the base for Case I and Case II, respectively, which are in the two different flow states. Lower pressure regions are observed in the proximity of vortex B as seen in figures 2(b) and 2(e), which show the torus of the pressure coefficient tilted in the streamwise direction, along with the line joining the vortex cores. In Case I, the bottom of the torus is farther away from the base, while in Case II, it is closer. Figure 2(e) also shows that the ground vortex spans approximately 50% of the width of the base. Shown in figures 2(c) and 2(f) are distribution of the (normalised) Reynolds normal stresses in the streamwise direction ($\langle u_x'^2 \rangle$). These figures show that the strongest intensity of the stresses occurs in the region associated with vortex C, and along the sides parallel to the longer edge of the model.

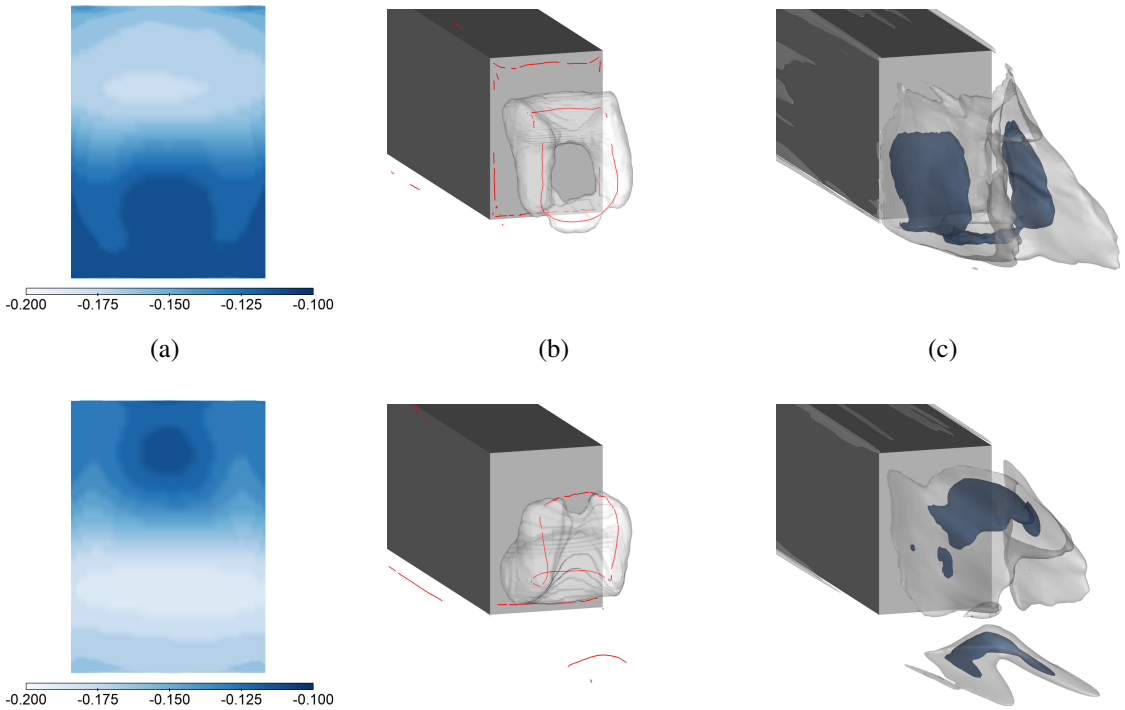

Figure 2: Top row: Case I; Bottom row: Case II. (a) and (d) Visualisation of the contours of the pressure coefficient on the base of the GTS. (b) and (e) Translucent isosurfaces of the pressure coefficient ($C_p = -0.2$) and the vortex cores are indicated by red lines. (c) and (f) Isosurfaces of the Reynolds normal stresses in the streamwise direction $\langle u_x'^2 \rangle$. White = 0.0375, blue = 0.02. Flow is from top left to bottom right in images (b), (c), (e) and (f).

3. Conclusions

The two flow states in the wake of a GTS are reproduced numerically by varying the turbulence models and the numerical schemes used for the momentum equations. While PANS-AVL SMART predicts a flow topology similar to the experimental work of [1, 2], PANS-CDS tends to predict a flow topology in the vertical midplane similar to that observed in the LES (cases III and IV) - which is anti-symmetric to the experiments with respect to the lateral midplane. PANS-CDS also requires a mesh of higher spatial resolution as compared to PANS-AVL SMART to accurately predict the detailed flow features, and results in an elongated recirculation region in the near wake as compared to other cases. The differences between the two flow states realisable in the wake of a GTS have now been identified based on the flow topology, pressure coefficient and the distribution of the streamwise Reynolds normal stresses.

The authors would like to thank the computational support provided by Chalmers Centre for Computational Science and Engineering (C3SE) and National Supercomputer Centre (NSC), Linköping University provided by the Swedish National Infrastructure for Computing (SNIC). The authors would also like to

acknowledge the support and licences provided by AVL GmbH, Austria.

References

[1] D. McArthur, D. Burton, M. C. Thompson, and J. Sheridan. On the near wake of a simplified heavy vehicle. *Journal of Fluids and Structures*, 66:293 – 314, 2016.

[2] B.L. Storms, J.C. Ross, J.T. Heineck, S.M. Walker, D.M. Driver, and G.G. Zilliac. An experimental study of the ground transportation system (GTS) model in the NASA Ames 7-by 10-ft wind tunnel. *National Aeronautics and Space Administration, Ames Research Center*, pages 1 – 21, 2001.

[3] S. Krajnović, R. Lárusson, and B. Basara. Superiority of PANS compared to LES in predicting a rudimentary landing gear flow with affordable meshes. *International Journal of Heat and Fluid Flow*, 37:109–122, 2012.

[4] B. Chaouat. The state of the art of hybrid RANS/LES modeling for the simulation of turbulent flows. *Flow, Turbulence and Combustion*, 99(2):279–327, Sep 2017.

[5] R. H. Croll, W. T. Gutierrez, B. Hassan, J. E. Suazo, and A. J. Riggins. Experimental investigation of the ground transportation systems (GTS) project for heavy vehicle drag reduction. In *SAE Technical Paper*. SAE International, 1996.

[6] C. Roy, J. Payne, and M. McWherter-Payne. RANS simulations of a simplified tractor/trailer geometry. *Journal of Fluids Engineering*, 128(5):1083–1089, 2006.

[7] R. Ghias, A. Khondge, and S. D. Sovani. Flow simulations around a generic ground transportation system: Using immersed boundary method. In *SAE Technical Paper*. SAE International, 2008.

[8] S. Girimaji and K. Abdol-Hamid. *Partially-Averaged Navier-Stokes Model for Turbulence: Implementation and Validation*, pages 1–14. American Institute of Aeronautics and Astronautics, Reno, Nevada, Jan 2005.

[9] B. Basara, S. Krajnović, S. S. Girimaji, and Z. Pavlovic. Near-wall formulation of the partially averaged Navier-Stokes turbulence model. *AIAA*, 49(12):2627–2636, 2011.

[10] G. Minelli, S. Krajnović, B. Basara, and B. R. Noack. Numerical investigation of active flow control around a generic truck A-pillar. *Flow, Turbulence and Combustion*, 97(4):1235–1254, Dec 2016.

[11] J. Östh and S. Krajnović. A LES study of a simplified tractor-trailer model. In *The Aerodynamics of Heavy Vehicles III*, pages 327–342. Springer, 2016.

[12] J. Östh and S. Krajnović. A study of the aerodynamics of a generic container freight wagon using Large-Eddy Simulation. *Journal of Fluids and Structures*, 44:31 – 51, 2014.

[13] A. Rao, G. Minelli, B. Basara, and S. Krajnović. On the two flow states in the wake of a hatchback Ahmed body. *Journal of Wind Engineering and Industrial Aerodynamics*, 173:262 – 278, 2018.

[14] M. Grandemange, M. Gohlke, and O. Cadot. Bi-stability in the turbulent wake past parallelepiped bodies with various aspect ratios and wall effects. *Physics of Fluids*, 25(9):095103, 2013.

[15] M. Grandemange, M. Gohlke, and O. Cadot. Turbulent wake past a three-dimensional blunt body. Part 1. Global modes and bi-stability. *Journal of Fluid Mechanics*, 722:5184, 2013.

[16] R. Volpe, V. Ferrand, A. D. Silva, and L. L. Moyne. Forces and flow structures evolution on a car body in a sudden crosswind. *Journal of Wind Engineering & Industrial Aerodynamics*, vol. 128:pp. 114–125, 2014.

[17] J.-M. Lucas, O. Cadot, V. Herbert, S. Parpais, and J. Délery. A numerical investigation of the asymmetric wake mode of a squareback Ahmed body effect of a base cavity. *Journal of Fluid Mechanics*, 831:675697, 2017.